RARE METALS

ORIGINAL ARTICLE

Microstructure and mechanical properties of TiAl/Ni-based superalloy joints vacuum brazed with Ti–Zr–Fe–Cu–Ni–Co–Mo filler metal

Bao Wan, Xiao-Qiang Li* , Cun-Liang Pan, Dong-Yu Li, Sheng-Guan Qu, Chao Yang

Abstract For the purpose of elevated temperature service and weight reduction in aerospace vehicle applications, a novel Ti–Zr–Fe–Cu–Ni–Co–Mo filler metal was employed to join TiAl to Ni-based superalloy (GH536). The effects of brazing temperature on interfacial microstructure and chemical composition of the joints were analyzed. The representative joint microstructure from TiAl substrate to GH536 substrate was primarily composed of four characteristic layers in order: B_2; Al_3NiTi_2; $AlNi_2Ti$ containing Cr-rich (Cr, Ni, Fe)$_{ss}$ (subscript ss represents solid solution), Ni-rich (Ni, Cr, Fe)$_{ss}$ and $TiNi_3$; Cr-rich (Cr, Ni, Fe)$_{ss}$ containing $AlNi_2Ti$, Ni-rich (Ni, Cr, Fe)$_{ss}$ and $TiNi_3$. Layer IV has the majority of the brazing seam, while Layer II was the thinnest. And the thickness of Layer II was not affected by brazing temperature. With the increase in brazing temperature in the range of 1110–1170 °C, both the shear strength and the thickness of brazing seam firstly increased and then decreased. The joint performance was jointly controlled by the thickness of brazing seam, the amounts of microcracks and intermetallic compounds formed in brazing seam. The maximum shear strength of 183 MPa at room temperature was obtained together with a peak thickness when the joint was brazed at 1150 °C for 10 min and the shear fracture mainly occurred in the thinnest Layer II Al_3NiTi_2.

Keywords TiAl alloy; Ni-based superalloy; Brazing; Microstructure; Shear strength

1 Introduction

The outstanding performance at elevated temperature makes intermetallic compounds attract a great deal of attention [1–3]. In particular, TiAl alloy is a promising structural material and has been widely employed in aerospace vehicle and automotive industry, due to its attractive properties of not only excellent creep resistance and good oxidation stability at elevated temperature, but also relatively low density and high specific strength [4–7]. Compared with Ni-based superalloy widely applied in the aviation field, TiAl alloy has many advantages such as quite lighter density (only half that of traditional Ni-based superalloy), better specific strength and higher specific stiffness, but its cost is much higher. So, TiAl alloy is often combined with Ni-based superalloy to obtain outstanding comprehensive performance accompanying with cost reduction. Therefore, joining of TiAl alloy to Ni-based superalloy to produce good performance dissimilar joints is of great interest to achieve the optimal material combination design.

However, due to the great differences in physical and chemical properties between TiAl alloy and Ni-based superalloy, joining them is a great challenge. First, due to that the dissolution enthalpy of Ti in liquid Ni solvent is up to $- 170$ kJ·mol^{-1} [8], many Ti–Ni intermetallic compounds, such as Ti_2Ni, $TiNi$ and $TiNi_3$, are prone to forming by the reaction of the Ti and Ni from the two base materials [9]. If the used filler metals cannot effectively restrain the Ti–Ni diffusion reaction between the parent materials, the formation of a large amount of intermetallic compounds will embrittle the joints and thus deteriorate the joint performance. Furthermore, the thermal expansion coefficient of Ni-based superalloy is much higher than that of TiAl alloy [10]. The difference will yield large residual

B. Wan, X.-Q. Li*, C.-L. Pan, D.-Y. Li, S.-G. Qu, C. Yang
National Engineering Research Center of Near-Net-Shape Forming for Metallic Materials, South China University of Technology, Guangzhou 510640, China
e-mail: Lixq@scut.edu.cn

stress in the brazed joints. Consequently, microcracks easily form in the joints which seriously weaken the joints strength. Therefore, joining TiAl alloy and Ni-based superalloy is an extremely difficult issue. It is very critical to inhibit the formation of brittle phase and to ensure favorable metallurgical quality at the joining interface.

At present, research on the joining of TiAl alloy to Ni-based superalloy mainly focuses on fusion welding [11], diffusion bonding [12–15] and brazing [16–19]. Traditional fusion welding method is difficult to obtain satisfactory joints, due to the obvious tendency of low-temperature brittleness and hot cracking mainly from TiAl alloy. Diffusion bonding and brazing are considered to be effective methods for joining TiAl alloy to Ni-based superalloy. But compared with diffusion bonding, brazing is in wide application in that it not only joins parts with complex shapes, but also has a simpler process [20, 21].

For the past few years, a few studies have been conducted on the brazing of TiAl alloy and Ni-based superalloy. Chen et al. [22] brazed the Ti_3Al alloy and GH536 with Ti–13Zr–21Cu–9Ni (wt%) filler metal. And due to the formation of many intermetallic compounds such as Ti–Ni and Ti–Fe in the brazing joints, the shear strength of the joints was low, only 86 MPa. Ren et al. [23] adopted Ag–21Cu–25Pd (wt%) filler metal to join Ti_3Al alloy and Ni-based superalloy under vacuum brazing. Pd mainly reacted with Ti_3Al substrate and formed intermetallic compounds of TiPd, Ti_3Pd_5 and AlPd. The joints brazed at 1253 K for 10 min presented the maximum tensile strength of 404 MPa at room temperature, and the tensile strength value of 212 MPa was maintained at 773 K. However, the filler is too expensive because of application of Ag and especially Pd.

In this study, vacuum brazing of TiAl alloy to GH536 alloy was done using a Ti–30Zr–10Fe–5Cu–4Ni–3Co–2Mo (wt%) filler metal. The microstructures of the dissimilar joints were analyzed in details. The effects of brazing temperature on the microstructural evolution and the mechanical properties of the joints were also investigated.

2 Experimental

2.1 Materials

The chemical compositions of TiAl and GH536 alloys used in this study are listed in Table 1. GH536 and TiAl alloys were machined into sizes of 22 mm × 6 mm × 3 mm and 5 mm × 6 mm × 3 mm, respectively. Brazing foil with a nominal composition of Ti–30Zr–10Fe–5Cu–4Ni–3Co–2Mo (wt%), which was 10 mm in width and 40 μm in thickness, was produced by rapid solidification technology in a vacuum single roller spinning quenching system (XC-

500). The melting temperature range of this brazing foil was 870–892 °C.

2.2 Brazing process

Prior to joining, all the joining surfaces were ground by up to 800-grit SiC paper, then cleaned ultrasonically in absolute ethyl alcohol and dried in air. The brazing foil was placed between the TiAl and GH536 specimens to form sandwich structure, as shown in Fig. 1a. During the brazing process, the assembly was placed into a graphite mold and a slight pressure was applied to ensure an appropriately close surface contact between the brazing filler and the substrates.

The brazing experiments were carried out in a HP-12 × 12 × 12 heating furnace with vacuum level up to 1.33×10^{-2} Pa. Figure 1b shows the heating process upon the brazing experiment. At the beginning of brazing process, the furnace was initially heated to 200 °C at a rate of 10 °C·min^{-1}. Afterward, the temperature was further increased to the brazing temperatures at higher heating rate of 20 °C·min^{-1} and the brazing temperature was set in the range of 1110–1170 °C and the brazing time was 10 min. Eventually, the specimens were cooled down to room temperature in the furnace.

2.3 Examination of structure and properties of joints

After brazing, the microstructures and fracture surfaces of the joints were characterized by a scanning electron microscope (SEM, Quanta 200) equipped with an energy dispersive X-ray spectrometer (EDS). Furthermore, the detailed microstructure of the joints was observed by a transmission electron microscope (TEM, FEI Tecnai F30) with selected area electron diffraction (SAED). The shear tests were conducted using a Shimadzu AG-X100KN universal material testing machine with a constant loading rate of 1 mm·min^{-1} at room temperature, as shown in Fig. 1c. The average joint shear strength of different brazing conditions was obtained from five tests. Nano-indentations were carried out with an Anton Paar, TTX-NHT3 to measure the hardness (H) and elastic modulus (E) of the joints. And the phases of fracture surface were identified by X-ray diffractometer (XRD, Bruker-AXS D8 Advance).
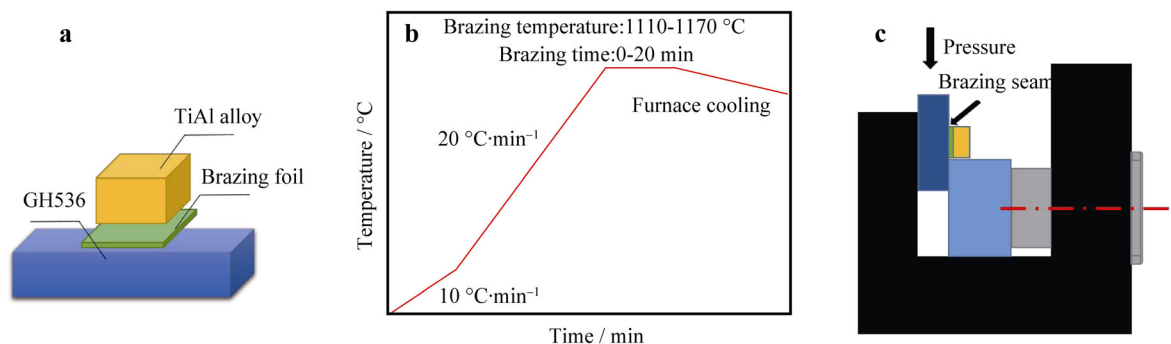
3 Results and discussion

3.1 Microstructural characterization of TiAl/GH536 joints

Figure 2 shows the typical interfacial microstructure of the joint brazed with Ti–Zr–Fe–Cu–Ni–Co–Mo filler metal at

Table 1 Chemical composition of TiAl and GH536 alloys (at%)

Alloys	Al	Ni	Cr	Ti	Nb	Fe	Co	Mo	W
TiAl	43.69	–	2.71	Bal	2.38	–	–	–	–
GH536	0.40	Bal	25.65	–	–	18.47	2.05	5.30	0.24

Fig. 1 a Schematic diagram for joining experiment; **b** heating curve for brazing process; **c** shear test of joint sample
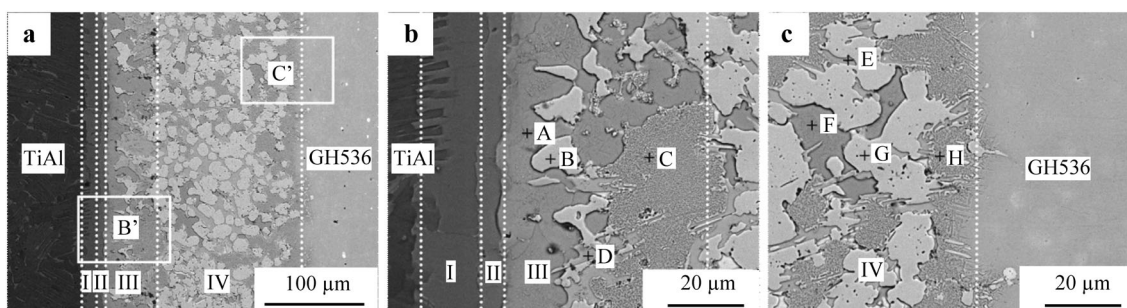
Fig. 2 SEM images of joint brazed at 1150 °C for 10 min: **a** joint; **b** high magnified image of Area B'; **c** high magnified image of Area C'

1150 °C for 10 min. As shown in Fig. 2a, the joint is soundly bonded and is devoid of imperfections such as cracks and voids. In addition, four different characteristic microstructures can be distinguished in the brazed joint based on their heterogeneous morphologies, which are marked as Layers I, II, III and IV. The four characteristic microstructures in turn from TiAl side to GH536 side are continuous diffusion Layer I, continuous isothermal solidification Layer II, reaction Layer III distributed with irregularity structure and reaction Layer IV distributed with island structure.

In order to verify the phase constitution in each layer, EDS analysis was carried out on the microstructure of the brazed joints. According to EDS results listed in Table 2, Layer I is mainly composed of Ti, Al and some β-Ti stable elements such as Cr, Nb and Mo. Combined with Ti–Al binary phase diagram [24], Layer I is referred as B_2 phase. Based on Table 2 and the Al–Ni–Ti ternary alloy phase diagram [25], Layer II can be deduced to be Al_3NiTi_2 phase, namely τ3 phase. Figure 2b, c shows that

there are four phases with different contrasts in Layers III and IV. The charcoal gray Phase A of Layer III is distributed continuously next to Layer II, the gray Phase C is flake, the white Phase B is island like, and the light gray Phase D is small strip. Different from Layer III, the charcoal gray Phase F of Layer IV is block. The gray Phase H presents continuous distribution next to GH536 substrate, but in local areas, it has island distribution. Furthermore, the white Phase G is the matrix in Layer IV, and the light gray Phase E presents strip like. The charcoal gray Phases A and F are mainly composed of Al, Ni and Ti, and the atomic ratio of Al, Ni and Ti is approximately equal to 1:2:1, which can be deduced to be $AlNi_2Ti$ phase, namely τ4 phase. In addition, the white Phases B and G are mainly composed of Cr, Fe and Ni, and the atomic ratio of Cr, Fe and Ni is close to 2:1:1, which can be inferred as Cr-rich $(Cr, Ni, Fe)_{ss}$ phase (subscript ss represents solid solution). The gray Phases C and H are mainly composed of Ni, Cr and Fe with an atomic ratio of 2:1:1, which can be inferred as Ni-rich $(Ni, Cr, Fe)_{ss}$ phases. Light grey Phases D and E

**Table 2** EDS chemical analysis results of different positions in Fig. 2 (at%)

Layer	Ti	Al	Ni	Cr	Fe	Zr	Cu	Nb	Co	Mo	Possible phase
I	56.86	34.23	1.64	3.25	1.36	0	0	2.47	0.15	0.04	B_2
II	33.75	38.90	17.70	3.28	3.53	0	0.36	1.94	0.43	0.11	Al_3NiTi_2
III											
Phase A	19.39	20.35	48.25	3.85	5.16	0.91	0.26	0.10	1.46	0.27	$AlNi_2Ti$
Phase B	3.42	2.14	19.14	40.61	20.53	0	0.10	0.00	2.01	12.05	Cr-rich (Cr, Ni, Fe)$_{ss}$
Phase C	7.37	4.33	41.36	20.06	21.35	0.18	0.42	0.20	2.05	2.68	Ni-rich (Ni, Cr, Fe)$_{ss}$
Phase D	16.65	5.01	61.88	4.71	7.14	1.30	0.45	0.55	1.71	0.60	$TiNi_3$
IV											
Phase E	18.37	4.15	63.39	3.81	5.96	1.28	0.69	0.23	1.74	0.38	$TiNi_3$
Phase F	18.44	18.44	48.91	4.79	5.71	0.89	0.50	0.34	1.45	0.53	$AlNi_2Ti$
Phase G	3.50	1.77	18.57	41.01	22.16	0.19	0.04	0.09	1.82	10.85	Cr-rich (Cr, Ni, Fe)$_{ss}$
Phase H	6.02	4.42	41.29	21.80	20.34	0.10	0.40	0.12	2.13	3.38	Ni-rich (Ni, Cr, Fe)$_{ss}$

are mainly composed of Ni and Ti, and the atomic ratio of Ni and Ti is approximately equal to 3:1. Referenced to Ti–Ni binary alloy phase diagram, it is deduced as $TiNi_3$ phase. The microstructure of Layers I, II and III was further verified by SAED, as shown in Fig. 3 (marked as Areas A–C). Combined with EDS results listed in Table 3, Areas A–C are further confirmed to be B_2, Al_3NiTi_2 and $AlNi_2Ti$.

Table 3 Chemical analysis results of different areas in Fig. 3 (at%)

Area	Al	Ti	Ni	Fe	Cr	Mo
A	37.63	57.03	0.71	1.13	3.50	0
B	41.64	33.27	18.04	3.30	3.64	0.11
C	25.14	23.12	45.60	5.24	0.37	0.53
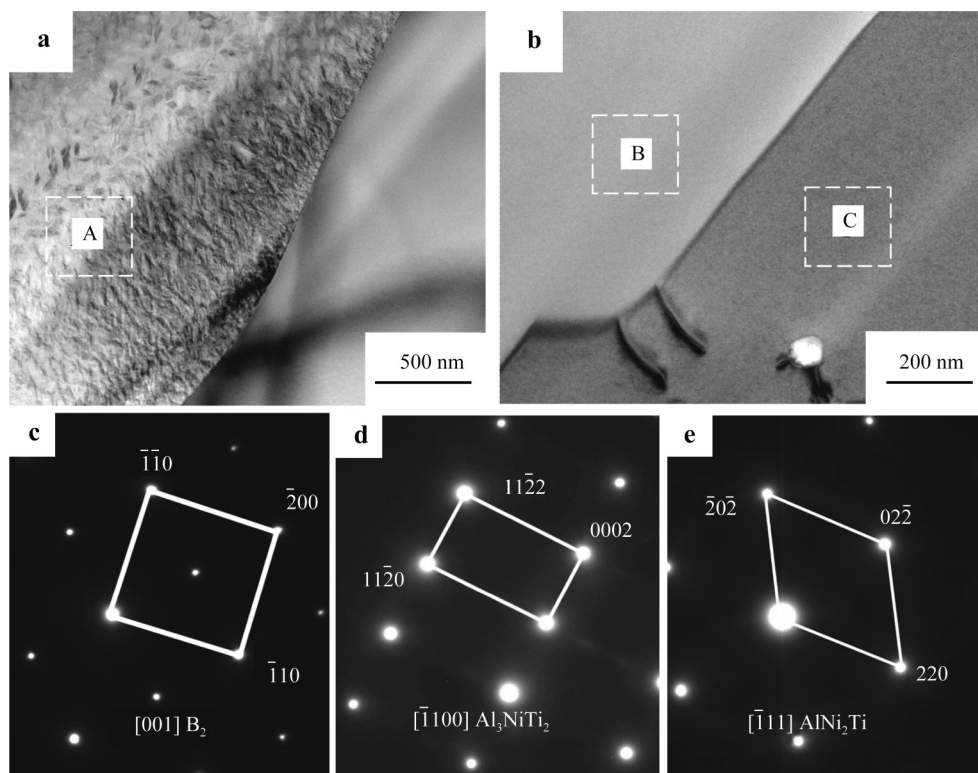
Fig. 3 TEM images of **a** Layer I and **b** Layer II–III; SAED patterns of **c** Area A in **a**, **d** Area B and **e** Area C in **b**
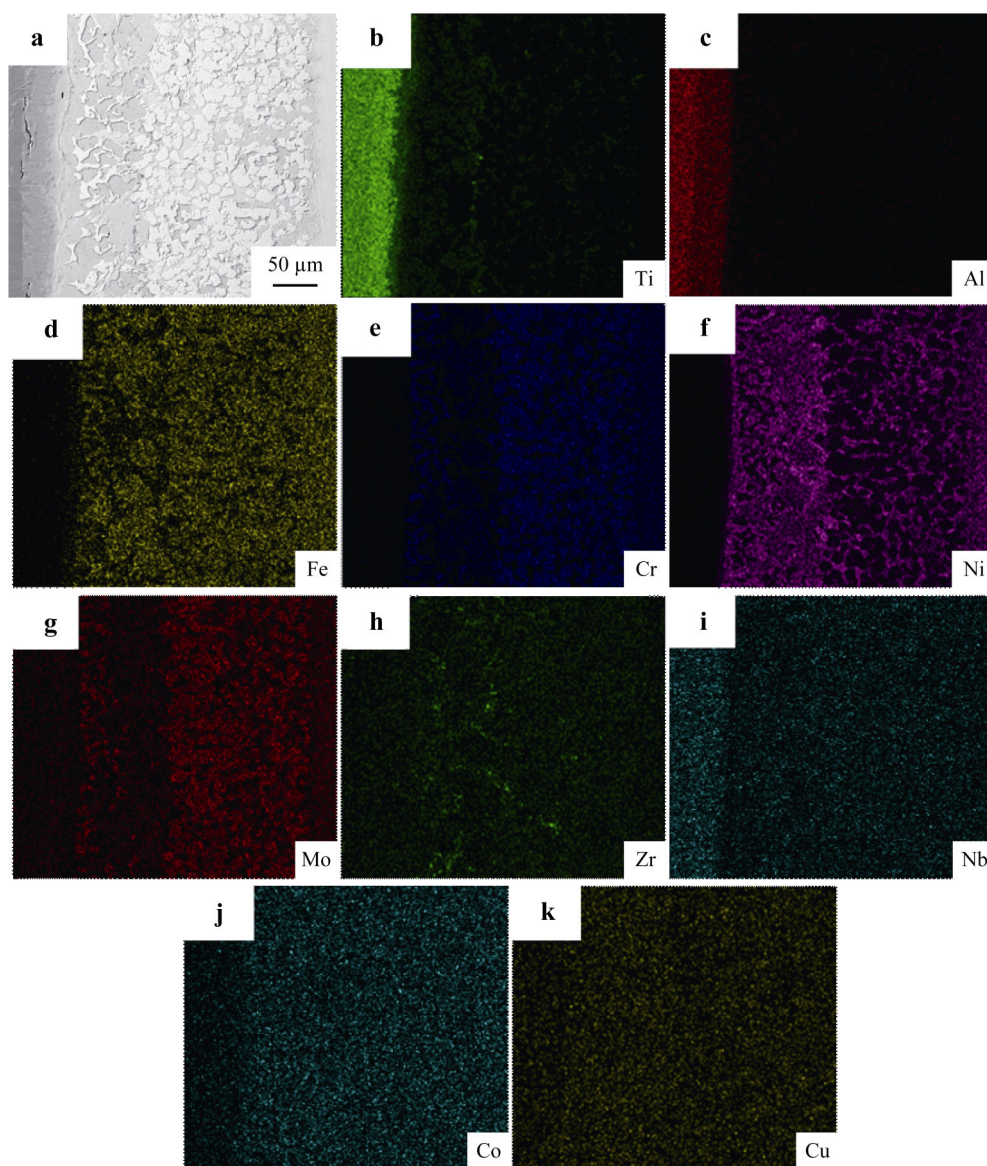
Fig. 4 **a** SEM image of joint brazed at 1150 °C for 10 min; corresponding elemental distribution maps of **b** Ti, **c** Al, **d** Fe, **e** Cr, **f** Ni, **g** Mo, **h** Zr, **i** Nb, **j** Co and **k** Cu

Figure 4 illustrates elemental distribution maps of the brazing seam of TiAl and GH536 alloys brazed at 1150 °C for 10 min. It can be seen that Ti, Al and Nb are mainly concentrated in Layers I, II and III. And the further the position is away from TiAl alloy substrate, the less the Ti, Al and Nb contents are. Cr, Ni and Fe are concentrated in Layers III and IV. In addition, Cr-rich and Ni-rich solid solutions can be clearly distinguished in Fig. 4d–f. As shown in Fig. 4g, the distribution of Mo is similar to that of Cr, and it can be judged that Mo is mainly distributed in Cr-rich (Cr, Ni, Fe)$_{ss}$. Zr lies mainly in Layer III and Co distributes uniformly in Layers III and IV. And the distribution of Cu is evenly in the brazing seam.

3.2 Microstructural evolution mechanism of joints

In order to describe the brazing process intuitively, a simplified schematic diagram of the microstructural evolution is proposed in Fig. 5. First of all, the filler metal begins to melt when brazing temperature exceeds its solidus temperature. Then, due to the concentration gradient, Al atoms diffuse from γ-TiAl substrate to the liquid filler metal and the out-diffusion of Al leads to the transformation of the original γ phase to B$_2$ phase of Layer I. Meanwhile, due to the diffusion of Ni, Cr and Fe from GH536 to the liquid filler metal, Ni-rich (Ni, Cr, Fe)$_{ss}$ Layer IV forms at filler/GH536 interface. With the increase in brazing temperature or holding time, Al and
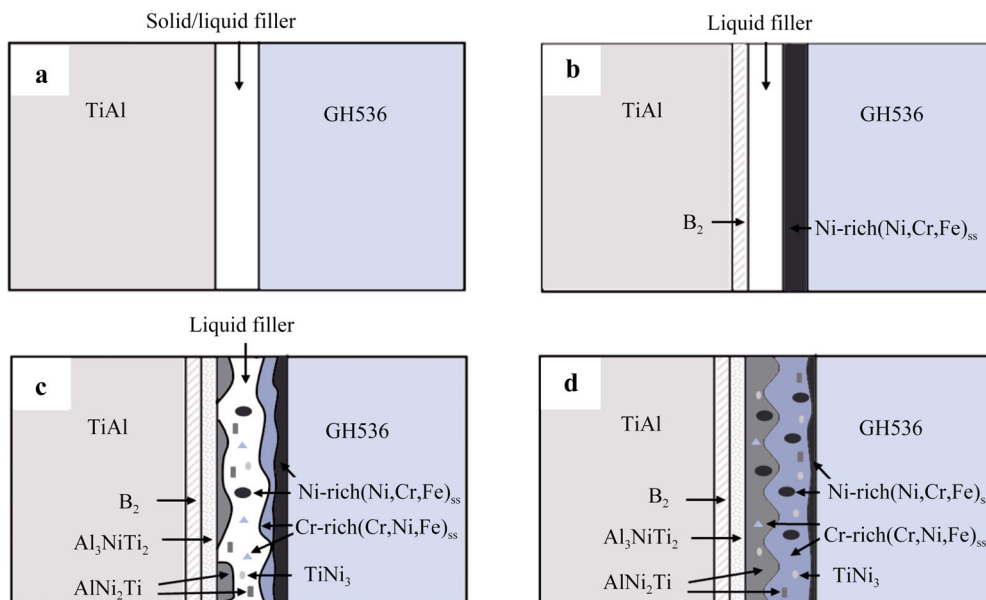
Fig. 5 Formation mechanism of microstructure of TiAl/GH536 joint: **a** filler melting; **b** formation of reaction layers B_2 and Ni-rich (Ni, Cr, Fe)$_{ss}$; **c** formation of Al$_3$NiTi$_2$, AlNi$_2$Ti, Cr-rich (Cr, Ni, Fe)$_{ss}$ phase; and **d** growth of reaction layers and reaction zone

Ni contents in the liquid filler gradually increase. Then, Al and Ni react with Ti in the liquid filler to form a thin layer of Al$_3$NiTi$_2$ phase next to B_2 phase. Under the effect of concentration gradient, Al in TiAl alloy and Ni in GH536 alloy further diffuse to the central area of the brazing seam. When the concentration increases to a certain extent, discontinuous AlNi$_2$Ti phase forms next to the Al$_3$NiTi$_2$ reaction Layer II. In the meantime, due to the further diffusion of Ni and Cr and the relatively increasing concentration of Cr, part of Ni-rich (Ni, Cr, Fe)$_{ss}$ turns to Cr-rich (Cr, Ni, Fe)$_{ss}$. Additionally, Ti in the liquid filler reacts with Ni, and a small amount of TiNi$_3$ phase is generated.

In the subsequent cooling stage, the residual liquid filler at the center of the brazing seam solidifies to form Layer III and the solid-state elemental diffusion in the brazed joint goes on. As a result of the mutual diffusion of elements, a few Cr-rich (Cr, Ni, Fe)$_{ss}$, Ni-rich (Ni, Cr, Fe)$_{ss}$ and TiNi$_3$ phases appear in AlNi2Ti reaction layer, while some Ni-rich (Ni, Cr, Fe)$_{ss}$, AlNi$_2$Ti and TiNi$_3$ phases also occur in the Cr-rich (Cr, Ni, Fe)$_{ss}$ matrix. Therefore, based on the above analysis, the typical interfacial microstructure of the joints brazed at 1150 °C for 10 min is composed of B_2, Al$_3$NiTi$_2$, AlNi$_2$Ti containing Cr-rich (Cr, Ni, Fe)$_{ss}$, Ni-rich (Ni, Cr, Fe)$_{ss}$ and TiNi$_3$, and Cr-rich (Cr, Ni, Fe)$_{ss}$ containing AlNi$_2$Ti, Ni-rich (Ni, Cr, Fe)$_{ss}$ and TiNi$_3$.

3.3 Effect of brazing temperature on microstructure of joint

Figure 6 shows the microstructure of the joints brazed at 1110, 1130, 1150 and 1170 °C for 10 min, respectively.

Due to insufficient metallurgical reaction and thermal stress in cooling, many microcracks can be observed in the brazing seam when the brazing temperature is 1110 °C, as shown in Fig. 6a. When the brazing temperature up to 1130 °C, the formation of microcracks in brazing seam has been suppressed to a certain extent, but it can still be easily observed. Such improvement is attributed to the increasing amount of Cr-rich (Cr, Ni, Fe)$_{ss}$ and Ni-rich (Ni, Cr, Fe)$_{ss}$ in the brazing seam and the decreasing amount of AlNi$_2$Ti, as shown in Fig. 6b. With the brazing temperature further increasing to 1150 and 1170 °C, the atomic interdiffusion can be accelerated, which causes metallurgical reaction more sufficient and no obvious defect in the brazing seam. In addition, the amount of AlNi$_2$Ti phase in the brazing seam significantly reduces; the grains of Cr-rich (Cr, Ni, Fe)$_{ss}$ and Ni-rich (Ni, Cr, Fe)$_{ss}$ become coarse, evenly scattering in island shape, as shown in Fig. 6c, d.

Figure 7 shows the thickness change trends of brazing seam and reaction layer with different brazing temperatures for 10 min. The total thickness of the brazing seam increases first and then decreases, and the peak value of 210 μm presents at 1150 °C. Actually, the thickness of the brazed joint is mainly determined by the dissolution of the two base metals and the loss of molten filler. The former will increase the joint thickness, and the later will play a role in reducing [26]. When the brazing temperature is below 1150 °C, the dissolution of the base metal plays a major role, which makes the brazing seam thicker with the temperature increasing. The fluidity of liquid filler is better at a higher brazing temperature such as 1170 °C. Thus, serious loss of filler arises, which results in the joint
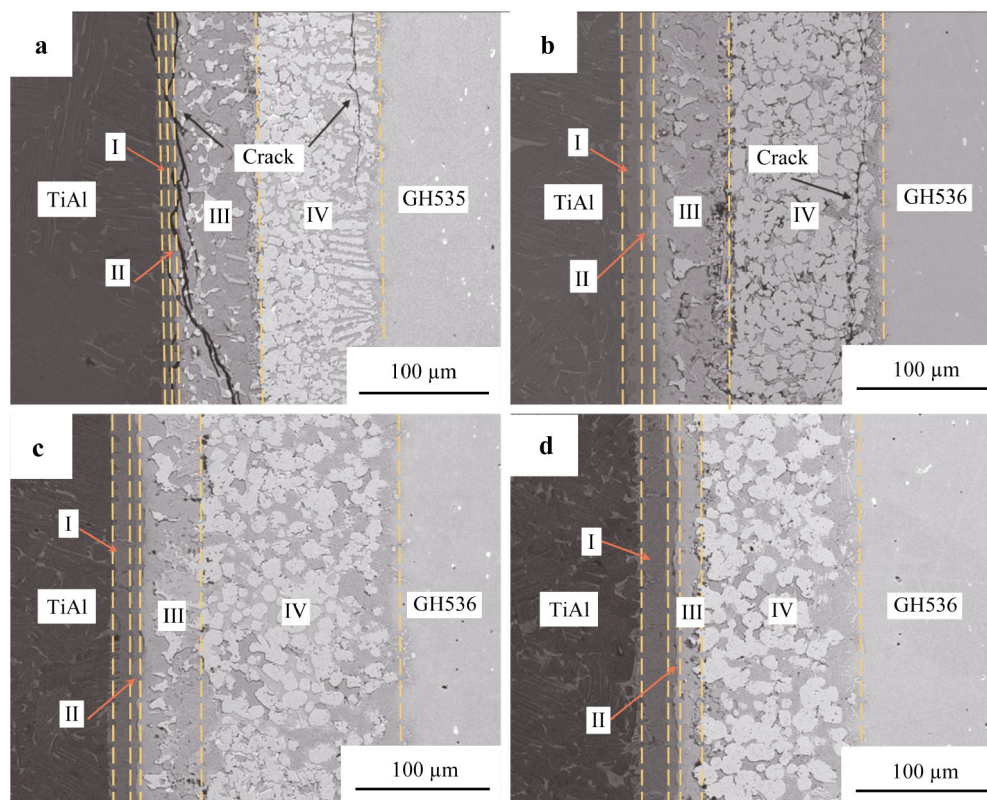
Fig. 6 SEM images of joints brazed at different temperatures for 10 min: **a** 1110 °C, **b** 1130 °C, **c** 1150 °C and **d** 1170 °C
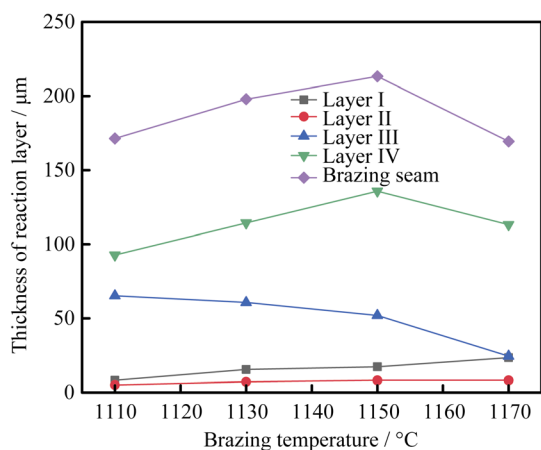

Fig. 7 Effect of brazing temperature on thickness of brazing seam and reaction layers

thickness reducing. Meanwhile, the increase in brazing temperature induces the thickness of Layers I and II increasing slightly. Once the continuous B_2 layer fully forms in the joint, the further atomic interdiffusion between TiAl alloy and filler metal would be suppressed. Furthermore, as the temperature rises, the formation of more Cr-rich $(Cr, Ni, Fe)_{ss}$ and Ni-rich $(Ni, Cr, Fe)_{ss}$ consumes a lot of Ni. Thus, the formation of $AlNi_2Ti$ phase reduces and the thickness of Layer III decreases consequently. In

addition, the thickness of Layer IV increases first and then decreases with a peak at 1150 °C. According to the previous analysis, it can be seen that the dissolution and diffusion of base metal causes the increase in thickness and the loss of filler results in the decrease of thickness. In the present research, the order of reaction layer thickness is Layer IV, Layer III, Layer I, Layer II from thick to thin. And Layer IV takes up the majority of brazing seam. In comparison with that of Layer IV, the thickness variation of Layer II can be overlooked.

3.4 Mechanical properties of TiAl/GH536 joints

Figure 8 displays the room-temperature shear strength of the joints brazed at 1110, 1130, 1150 and 1170 °C for 10 min, respectively. The strength has a similar trend to the total thickness of brazing seam with the increase in brazing temperature. At a lower brazing temperature, the fluidity of the liquid filler is poor and the dissolution and reaction between the substrates and the liquid filler are insufficient, which results in that the thickness of the brazing seam is relatively thin and appropriate interfacial reaction layers are not formed. In addition, the amount of $AlNi_2Ti$ phase in Layer III is relatively larger and the formation of overmuch intermetallic compounds leads to microcracks present in the joint, so a relatively low strength will be obtained (e.g.,
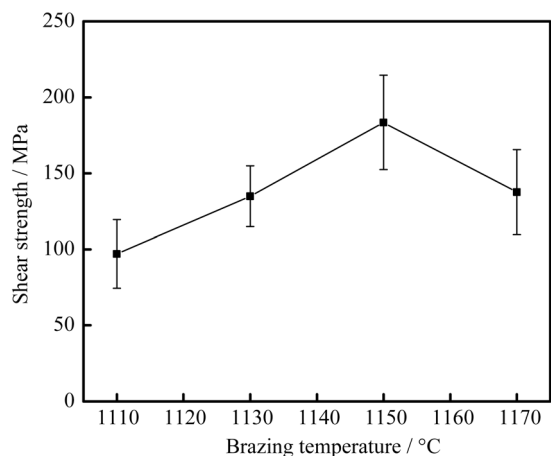
Fig. 8 Shear strength of joints brazed at different temperatures for 10 min

97 MPa for 1110 °C). With the brazing temperature up to 1130 °C, the joint strength is improved to 135 MPa. It can be attributed to the increase in brazing seam thickness, the decrease in the amount of $AlNi_2Ti$ phase in Layer III and the depression of the microcracks in the brazing seam. When the brazing temperature is 1150 °C and the brazing seam thickness reaches the maximum, which indicates better metallurgic bonding in the joint. As a result, the shear strength further goes up to 183 MPa. Generally, a too wide joint thickness will lead to dramatical deterioration of bonding strength [27, 28]. However, in the present work, the joint strength and thickness reach the maximum synchronously. Too high brazing temperature leads to severe loss of filler metal and higher residual stress [29]. The continuous reaction Layer III becomes thinner and unable

to bear a large load [30]. Accordingly, the shear strength decreases instead at 1170 °C.

Although different brazing temperatures yield different joint shear strengths, there are similar fracture paths and fracture morphology in the brazing temperature range of 1110–1170 °C, due to the formation of similar joint microstructure except for the thickness of reaction layers and microcracks. As shown in Fig. 9a, the joint brazed at 1150 °C for 10 min breaks mainly in Layer II, and the microcracks originate from Layer II and then gradually propagate to Layers I and III. According to the elastic modulus (E) and hardness (H) results listed in Table 4, Al_3NiTi_2 phase has the highest E and H in the brazing seam, which suggests that the plasticity of Layer II is the worst. And the microstructure of Layer IV mainly consists of Cr-rich (Cr, Ni, Fe)$_{ss}$ and Ni-rich (Ni, Cr, Fe)$_{ss}$, which could restrain the crack propagation due to their excellent plasticity. Therefore, the crack tends to propagate in Layer II during the shear test. The fracture surface is microscopically flat and exhibits a cleavage fracture feature with river pattern. From XRD pattern of the fracture surfaces, it is further confirmed that the main phase on the fracture surface is Al_3NiTi_2 intermetallic compound. Accordingly, it is also confirmed that Layer II primarily consisting of brittle Al_3NiTi_2 intermetallic compound is the weakest area in the joint.

4 Conclusion

Vacuum brazing of joining TiAl alloy to GH536 alloy was successfully achieved by using Ti–Zr–Fe–Cu–Ni–Co–Mo
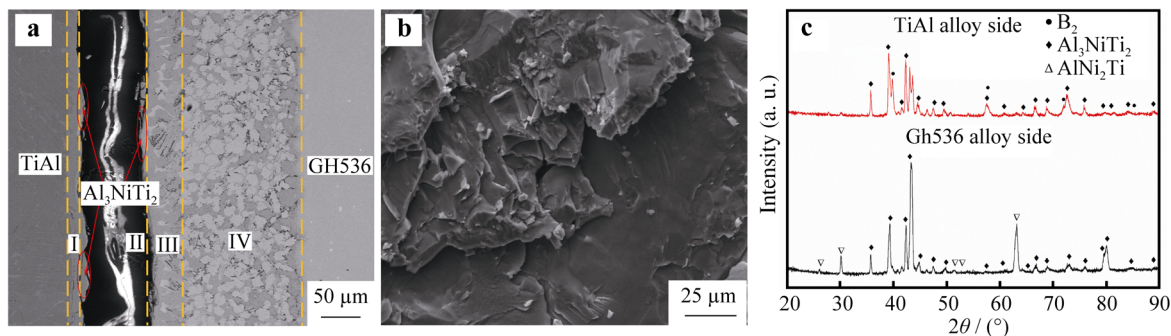
Fig. 9 **a** Fracture path, **b** fracture surface and **c** XRD patterns of fracture surface of joint brazed at 1150 °C for 10 min

Table 4 Mechanical properties of reaction phases in brazed joint

Phase	γ-TiAl	B_2	Al_3NiTi_2	$AlNi_2Ti$	Cr-rich (Cr, Ni, Fe)$_{ss}$	Ni-rich (Ni, Cr, Fe)$_{ss}$	GH536
Modulus/GPa	147.436	149.729	267.595	172.648	239.275	181.763	158.064
Hardness/GPa	4.867	9.328	17.152	9.759	14.979	5.864	4.180

filler metal. The interfacial microstructure and mechanical properties of the brazed joints were investigated in details. Experimental results show that the representative joint microstructure from TiAl substrate to GH536 substrate is primarily composed of four characteristic layers in order: B_2; Al_3NiTi_2; $AlNi_2Ti$ containing Cr-rich $(Cr, Ni, Fe)_{ss}$, Ni-rich $(Ni, Cr, Fe)_{ss}$ and $TiNi_3$; Cr-rich $(Cr, Ni, Fe)_{ss}$ containing $AlNi_2Ti$, Ni-rich $(Ni, Cr, Fe)_{ss}$ and $TiNi_3$.

With the increase in brazing temperature in the range of 1110–1170 °C, the thickness of brazing seam firstly increases and then decreases, reaching its peak at 1150 °C. Layer IV is the majority of the brazing seam, while Layer II is the thinnest. And the thickness of Layer II is not affected by brazing temperature. The shear strength of the joints increases first and then decreases with the increase in the brazing temperature. The joint brazed at 1150 °C for 10 min obtains the maximum shear strength of 183 MPa. Brazed joints break mainly in Layer II because of the worst plasticity of Al_3NiTi_2. The fracture surface shows typical cleavage fracture characteristics, and the crack originates from Layer II and then gradually propagates to Layers I and III.

References

[1] Cai YS, Liu RC, Zhu ZW, Cui YY, Yang R. Effect of brazing temperature and brazing time on the microstructure and tensile strength of TiAl-based alloy joints with Ti–Zr–Cu–Ni amorphous alloy as filler metal. Intermetallics. 2017;91:35.

[2] Zhang TT, Yang XS, Miao KS, Li DY, Chen S, Cui XP, Huang M. Microstructure evolution and brazing mechanism of Ti_5Si_3/Ti_3Al composite and Ni-based superalloy joints using Ti–Zr–Cu–Ni filler alloy. Mater Sci Eng A. 2018;713:28.

[3] Li L, Li XQ, Li ZF, Zhu DZ, Qu SG. Characterization of Ti–Zr–Cu–Ni–Co–Mo filler and brazed γ-TiAl joint. Rare Met Mater Eng. 2017;46(08):2214.

[4] Wu Y, Liu Y, Li C, Xia X, Wu J, Li H. Coarsening behavior of γ′ precipitates in the γ′ + γ area of a Ni_3Al-based alloy. J Alloys Compd. 2019;771:526.

[5] Huang Y, Liu Y, Li C, Ma Z, Yu L, Li H. Microstructure evolution and phase transformations in Ti–22Al–25Nb alloys tailored by super-transus solution treatment. Vacuum. 2019;161:209.

[6] Zhang WJ, Song XY, Hui SX, Ye WJ, Wang WQ. Phase precipitation behavior and tensile property of a Ti–Al–Sn–Zr–Mo–Nb–W–Si titanium alloy. Rare Met. 2018;36(12):1064.

[7] Yang Y, Chen RR, Fang HZ, Guo JJ, Ding HS, Su YQ, Fu HZ. Improving microstructure and mechanical properties of Ti43Al5Nb0.1B alloy by addition of Fe. Rare Met. 2019;36(11):1024.

[8] Miedema AR, Boer FRDE, Boom R, Dorleijn JWF. Model predictions for the enthalpy of formation of transition metal alloys. Calphad. 1977;1(4):341.

[9] Keyzer JD, Cacciamani G, Dupin N, Wollants P. Thermodynamic modeling and optimization of the Fe–Ni–Ti system. Calphad. 2009;33(1):109.

[10] Ren HS, Xiong HP, Wu X, Chen B, Cheng YY, Chen BQ. Research progress of dissimilar joining technology between Ti–Al alloy and Ni-based superalloy. J Mech Eng. 2017;53(04):1.

[11] Cai XL, Sun DQ, Li HM, Meng C, Wang L, Shen CJ. Dissimilar joining of TiAl alloy and Ni-based superalloy by laser welding technology using V/Cu composite interlayer. Opt Laser Technol. 2019;111:205.

[12] Luo GX, Wu GQ, Huang Z, Ruan ZJ. Diffusion bonding of laser-surface-modified gamma titanium aluminide alloy to nickel-based casting alloy. Scr Mater. 2007;57(6):521.

[13] He P, Wang J, Lin TS, Li HX. Effect of hydrogen on diffusion bonding of TiAl-based intermetallics and Ni-based superalloy using hydrogenated Ti6Al4V interlayer. Intermet J Hydrogen Energy. 2014;39(4):1882.

[14] Li ZF, Wu GQ, Huang Z, Ruan ZJ. Diffusion bonding of laser surface modified TiAl alloy/Ni alloy. Mater Lett. 2004;58(27–28):3470.

[15] Dong KW, Kong J, Wei ZX, Yang Y, Liang YL, Peng Y, Zhou Q, Wang KH. Thermoplastic bonding (TPB) of TiAl- and Ni-based alloys with Zr–Al–Ni–Cu bulk metallic glass. Mater Des. 2019;181:107936.

[16] Li HX, Wei HM, He P, Lin TS, Feng JC, Huang YD. Effects of alloying elements in GH99 superalloy on microstructure evolution of reactive brazing TiAl/GH99 joints. Intermetallics. 2013;34:69.

[17] Tetsui T. Effects of brazing filler on properties of brazed joints between TiAl and metallic materials. Intermetallics. 2001;9(3):253.

[18] Dong KW, Kong J. A high-strength vacuum-brazed TiAl/Ni joint at room temperature and high temperature with an amorphous foil Zr–Al–Ni–Co filler metal. J Manuf Process. 2019;44:389.

[19] He P, Li HX, Lin TS, Feng JC. Interfacial microstructure and properties of brazing joints of TiAl/Ni-based alloy. Rare Met Mater Eng. 2013;42(11):2248.

[20] He P, Feng JC, Zhou H. Microstructure and strength of brazed joints of Ti_3Al-basealloy with NiCrSiB. Mater Charact. 2004;52(4):309.

[21] Shiue RK, Wu SK, Chen SY. Infrared brazing of TiAl intermetallic using BAg-8 braze alloy. Acta Mater. 2003;51(7):1991.

[22] Chen B, Xiong HP, Mao W, Cheng YY. Microstructures and properties of Ti_3Al/Ti_3Al and Ti_3Al/GH536 joints using Ti–Zr–Cu–Ni brazing filler. J Aeronaut Mater. 2010;30(5):35.

[23] Ren HS, Xiong HP, Long WM, Shen YX, Pang SJ, Chen B, Cheng YY. Interfacial diffusion reactions and mechanical properties of Ti_3Al/Ni-based superalloy joints brazed with AgCuPd filler metal. Mater Charact. 2018;144:316.

[24] Jung IS, Kim MC, Lee JH. High temperature phase equilibria near Ti-50at%Al composition in Ti–Al system studied by directional solidification. Intermetallics. 1999;7(11):1247.

[25] Schuster JC, Pan Z, Liu SH, Weitzer F, Du Y. On the constitution of the ternary system Al–Ni–Ti. Intermetallics. 2007;15(9):1257.

[26] Li HX, Lin TS, He P, Wang XJ, Feng JC. Interfacial microstructure and properties of TiAl–Ni based alloy contact reaction brazed joint. Rare Met Mater Eng. 2012;41(11):1945.

[27] Feng JC, Dai XY, Wang D, Li R, Cao J. Microstructure evolution and mechanical properties of ZrO_2/TiAl joints vacuum brazed by Ag–Cu filler metal. Mater Sci Eng A. 2015;639:739.

[28] Zhang J, Zhang Q, Liu CF, Wang GC, Xuan YH. Effect of brazing temperature on microstructure and mechanical properties of 2D Cf/SiC and Nb joints brazed with Co–Ti–Nb filler alloy. Mater Sci Eng A. 2015;634:116.

[29] Akselsen OM. Advances in brazing of ceramics. J Mater Sci. 1992;27(8):1989.

[30] Zhang J, He YM, Sun Y, Liu CF. Microstructure evolution of Si_3N_4/Si_3N_4 joint brazed with Ag–Cu–Ti + SiCp composite filler. Ceram Int. 2010;36(4):1397.